

The CIDA-UCM-Yale Shallow Survey for Emission Line Galaxies

A. Bongiovanni¹*, G. Bruzual¹, G. Magris¹, J. Gallego², C.E. García-Dabó², P. Coppi³, C. Sabbey⁴

¹Centro de Investigaciones de Astronomía, CIDA, AP 264, Mérida 5101-A, Venezuela

²Universidad Complutense de Madrid, Departamento de Astrofísica y Ciencias de la Atmósfera, Facultad de Ciencias Físicas, Madrid, España

³Yale University, Astronomy Department, P.O. Box 208101, New Haven, CT 06520, USA

⁴Bogle Investment Management, Wellesley, MA 02481, USA

Accepted ... Received ...; in original form ...

ABSTRACT

We present the CIDA-UCM-Yale (Centro de Investigaciones de Astronomía, Universidad Complutense de Madrid and Yale University) survey for H α + [NII]6549, 6584 emission-line galaxies using objective-prism spectra. The most important properties of a catalogue with 427 entries and significant subsets are analysed. The complete sample contains 183 statistically confirmed ELGs in a sky area of 151 deg² and redshift up to 0.14. We determine the parameters of the H α luminosity function using the H α + [NII] flux directly measured on the ELGs spectra in this sample and the star formation rate density derived is in agreement with the values reported in the literature. Finally, we study the clustering properties of local star-forming galaxies relative to quiescent ones from different perspectives. We find that emission-line galaxies avoid dense regions of quiescent galaxies and we propose a power-law expression to parametrise the relation between star formation rate density and environment volume density of emission-line galaxies.

Key words: surveys - galaxies: luminosity function, star formation - cosmology: large scale structure

1 INTRODUCTION

The star formation rate density (ρ_{SFR}) in the Local Universe and the spatial distribution of emission-line galaxies (ELGs) as a function of environment are fundamental pieces in the field of formation and evolution of galaxies. There are few techniques as good as slitless spectroscopy for bulk-searching of this object class. From the mid 1960s to the near past the photographic plates were used as unique detectors in the search on ELGs (e.g. MacAlpine, Smith & Lewis 1977; Wasilewski 1983; Pesch & Sanduleak 1983; Markarian, Stepanian & Erastova 1986; Popescu et al. 1996; Surace & Comte 1998 and references therein; Ugrumov et al. 1999). The UCM (Universidad Complutense de Madrid) survey (Zamorano et al. 1994) is one of the more recent initiatives devoted to the photographic searching of ELGs and their findings motivated this work. Substitution of photographic plates by large-format CCDs, including CCD mosaics, is re-

ally a challenge for many observatories with competitive aperture Schmidt telescopes, some of them equipped with objective-prisms. Consequently, the CCD-based objective-prism surveys could be taken as a promising technique for the search of extragalactic emission-line systems. Examples of two successful objective-prism digital surveys are presented by (Sabbey et al. 2001) and (Gronwall et al. 2004, and references therein, hereafter KR2), the latter best known as the KPNO international spectroscopic survey, KISS.

The CIDA-UCM-Yale (Centro de Investigaciones de Astronomía, Universidad Complutense de Madrid and Yale University) survey¹, hereafter CUYS, is the first stage of an observational effort with the main goal of identifying

¹ The data presented here were partially extracted from the QUEST1 Collaboration raw data repository. QUEST1 is short for the Quasar Equatorial Survey Team, and it was the first collaboration between groups from Yale University, Indiana University, Centro de Investigaciones de Astronomía (CIDA), and Universidad de Los Andes (Mérida, Venezuela).

and studying emission-line galaxies (ELGs) based on digital low-resolution spectra in contrast with spectroscopic surveys which involve follow-up observations or multifiber instruments. Once the second part of this equatorial objective-prism survey is completed, we expect to have catalogued more than 10,000 ELGs with blue and red low-resolution spectra (4,000-9,200 Å) over ~ 600 deg 2 . The CUYS is being carried out in the 1m Schmidt telescope located at the Venezuelan National Astronomical Observatory, Llano del Hato, Mérida, Venezuela ². This telescope is equipped with a 3.4° objective-prism (reciprocal dispersion ~ 25 Å arcsec $^{-1}$ in H α at rest) and a 4×4 CCD mosaic covering $2.3^\circ \times 3.5^\circ$ on the sky. The CCDs are 2048×2048 LORAL devices with $15\mu\text{m}$ pixels. The camera and its operation details are fully described in Baltay et al. (2002).

Our strategy to select ELGs is the detection of H α + [NII]6549, 6584 Å emission on reduced 1-dimensional spectra of extended sources listed in the APM catalogue (Irwin 1990). Because objective-prism dispersion decreases in the red portion of the spectra, absorption bands present in late-type star spectra could generate false emission line detections. To avoid these contaminants, among others, we chose to ignore the spectra of point-like sources. Taking into account the galactic latitude range of the CUYS observations, data reduction allowed us to obtain a statistically complete catalogue of active star-forming galaxies and to study the spatial distribution of these objects on medium and large scales (above ~ 3 Mpc). Several approaches have been used to study this topic during the last 15 years. It is well established that ELGs can be found near structures defined by luminous normal galaxies (Schechter 1976) or populating low galaxy density regions in the nearby universe (Popescu, Hopp & Elsaesser 1997). Consequently, there is a relation between mean star formation rate (SFR) and environment in the sense that ρ_{SFR} decreases as the galaxy number density increases (e.g. Gisler 1978, Dressler, Thompson & Schechter 1985, Lewis et al. 2002). Recently, Gómez et al. (2003) have established an inverse relation between environmental surface density and SFR measured using ELGs from the SDSS. A plausible explanation is that the high mean SFR in low density environments of the local universe is only a contrast effect resulting from the mild SFR in high density regions in which galaxies are stripped of their gas with more probability.

This paper is organized as follows. An analysis of the catalogue properties is the aim of section 2. In section 3 we use the resulting CUYS ELG catalogue to find the parameters of the H α Luminosity Function (LF) and estimate the ρ_{SFR} in the Local Universe using fluxes and equivalent widths (EW) measured directly from objective-prism spectra. In section 4 we analyse the spatial distribution of ELGs in our survey in terms of the 2-point correlation function and other statistical estimators related to the spatial distribution at large scales. We conclude in section 5. Throughout this paper, we adopt the standard notation $h = H_0/100$ km s $^{-1}$ Mpc $^{-1}$ and the cosmology $\Omega_m = 0.3$ and $\Omega_\Lambda = 0.7$, nevertheless the latter assumption has not much effect on the redshift range of our survey.

² Operated by CIDA and funded by the Ministerio de Ciencia y Tecnología, Venezuela.

2 SURVEY DESCRIPTION

2.1 Observations

Observations were performed in the second half of 1999 and the beginning of 2000 with the instruments described above. The use of a red cut-off filter (6300-9200 Å) allowed us to minimize the overlapping of spectra, especially in crowded zones, profiting at the same time from the CCDs best response in this wavelength range. This instrumental combination limits the H α +[NII] detection in redshift to $z \leq 0.4$. Data were collected using the driftscan technique, which is also referred to as time-delay integration mode (McGraw, Cawson & Keane 1986). From 23 scans (~ 0.21 Tbytes) we selected the best 18 (which covered repeatedly almost the same regions). We detect objects with continuum magnitudes down to $R \sim 20$. These scans cover the equatorial sky between coordinates $08h \leq \alpha \leq 18h$ and $-2.4^\circ \leq \delta \leq +0.1^\circ$. From the surveyed region, we selected the best sampled zones, which represent about 250 deg 2 . The different atmospheric conditions prevailing during the observing nights and the artificial broadening of the spectra introduced by the driftscan mode (produced by residual effects due to the motion of the spectral sagitta and spread in the rate of motion of spectra across the finite width of a single CCD, Baltay et al. 2002), result in an average full width at half maximum ($fwhm$) of the spectra of ~ 3 arcsec in the spatial direction.

2.2 Data Reduction

To process the observations we used the objective-prism data analysis package from Sabbe (1999), in a version modified by the authors. We omit a detailed description of this package and only mention the more important steps of the analysis. (a) Extraction of the astrometric database from the USNO-A V2.0 catalogue (Monet et al. 1998) for object identification; (b) Generation of calibration files (bias level, flat field vector and bad column list) for each CCD; (c) Determination of linear coordinate transformation between the astrometric database and the driftscan strip world coordinates. We used the centroid of the telluric A band (O₂, 7580-7750 Å) as a reference to guide the positioning of the spectra in one of the image axis; (d) Extraction of wavelength calibrated 1-dimensional spectra for each object identified in the USNO-A V2.0 catalogue; (e) Coaddition of 1-dimensional spectra (four for each driftscan, i.e. 560 s of integration time) in a database created for this purpose, which also provides information to discard cosmic rays; (f) Extraction of raw ELG candidates applying an optimal emission line detection algorithm; (g) Flux calibration and analysis of ELG candidate spectra that matched with the previous selection of sources identified as extended in the b_J - and r -band digitized images of the APM catalogue to discard possible contaminants in the light of the CUYS goals, i.e. late-type stars and QSOs. (h) Finally, study of the 1-D spectra of selected candidates, using the Image Reduction and Analysis Facility (IRAF³) software. About this data reduc-

³ IRAF is distributed by the National Astronomical Observatory, which is operated by the Association of Universities for Research in Astronomy, Inc. (AURA), under cooperative agreement with the National Science Foundation (USA).

Table 1. List of the first 10 entries in the CUYS catalogue. Right ascension, declination and R magnitude were extracted from the USNO-A V2.0 catalogue. The redshift, equivalent width [Å] and H α +[NII] flux [erg s $^{-1}$ cm $^{-2}$], were measured directly on the CUYS objective-prism spectra.

Object Name	R.A.(J2000.0)	Dec.(J2000.0)	R	Redshift	EW(H α +[NII])	log flux(H α +[NII])
CUYS 091452-003359	09:14:52.40	-00:33:58.79	15.18	0.060	25.3	-14.45
CUYS 091955-005953	09:19:55.32	-00:59:52.58	14.68	0.097	32.1	-14.06
CUYS 092244-001853	09:22:44.76	-00:18:52.20	15.55	0.057	17.2	-15.35
CUYS 092439-010238	09:24:39.57	-01:02:37.90	18.75	0.302	105.0	-14.04
CUYS 092440-000049	09:24:40.18	-00:00:48.13	14.35	0.064	66.2	-13.90
CUYS 092551-020918	09:25:51.51	-02:09:18.90	17.66	0.268	72.9	-14.01
CUYS 092552-012438	09:25:52.02	-01:24:38.74	14.91	0.076	51.4	-13.96
CUYS 093235-010234	09:32:35.74	-01:02:33.72	16.44	0.226	31.5	-13.94
CUYS 093343-013256	09:33:43.95	-01:32:56.62	16.13	0.081	83.7	-13.79
CUYS 093448-003108	09:34:48.33	-00:31:07.82	15.92	0.102	56.3	-13.90

tion scheme, the explanations that follow could be useful to the reader.

Because the objective-prism dispersion decrease in the red portion of the spectrum, the absorption bands present in late-type stars spectra could generate false emission line detections. To avoid this we chose to rule out APM point-like sources spectra and only use the confirmed APM extended and paired sources. Taking into account the coverage of the CUYS in galactic latitude (from $\sim 30^\circ$ to 62°), we discard between 1390 to 3420 K and M type stars deg $^{-2}$; these quantities were calculated using the Bahcall & Soneira (1980) model. Additionally, we estimate that nearly 4-5 QSO deg $^{-2}$ (Crawford 1995) are rejected before any data processing effort using this method. Conversely, our method introduces a bias against very compact ELGs: near 8 per cent of *star-like* ELGs were found in the UCM survey list 3 sample and 11 per cent were morphologically classified as *compact* ELGs (Alonso et al. 1999). Obviously, this bias did not affect the UCM survey. In absence of simulations better qualified than this observational fact, we presume that 30 to 40 ELGs in the final CUYS catalogue were lost due to the selection effect introduced by excluding *star-like* ELG candidates presumably included in the set of point-like sources initially ignored. These numbers demonstrate the advantage of point-like source rejection as a previous step to the individual ELGs candidates processing, in spite of the bias described. This acquires special relevance when the follow-up spectroscopy is not foreseen in the original observational project.

With respect to the flux calibration, it was carried out using the optical continuum of 15 AGNs spectra observed at the 2.5 m DuPont telescope by Sabbe (2001, unpublished), and included in the CUYS catalogue, to construct the average sensitivity curve for each column of the CCD mosaic. Such curves were used for the flux calibration of the CUYS spectra. The sensitivity curve reliability was double-checked using the colour-selected F8 sub-dwarf secondary standards spectra obtained from the SDSS Data Release 2 (Abazajian et al. 2003, hereafter SDSS2) instead of AGNs spectra. These standards were originally used in the SDSS for their spectra calibration. Previously, we ruled out those secondary standards with known photometric variability in periods from days to years, using data from the QUEST RR Lyrae Survey (Vivas et al. 2004, hereafter QRR). The

resulting sensitivity curves are consistent (1σ) with those obtained using AGN continua.

Finally, the extraction of raw ELG candidates followed the combination of three different criteria: The *S/N* ratio, the *fw* and the observed *EW* of emission lines on each spectrum. Several experiments were performed to achieve optimum values and a balance between completeness and low contamination. The result was a step function of observed *EW* and emission line *S/N* ratio for candidate selection. An $EW \approx 40$ Å and emission line *S/N* ≈ 4 were adopted as initial security thresholds. Above these values it is possible to avoid false emission detections (Schneider, Schmidt & Gunn 1994). Once cosmic rays were discarded and additional criteria for physical emission confirmation were applied, the spectra were subject to a final visual inspection. The completeness analysis below demonstrates that the application of these criteria allowed us to create a statistically significant catalogue of ELGs.

2.3 Survey Results

The CUYS results are presented as a catalogue of ELGs. The entire catalogue can be inspected in the CIDA homepage.⁵ It contains 427 entries and a summary of the first 10 is listed in Table 1. Astrometric positions (J2000.0) and R magnitudes of the ELG candidates were extracted from the USNO-A V2.0 catalogue. Instrumental photometry (*V* and *R* Johnson-Cousins bands) from QRR for 73.5 per cent (314 objects) of the catalogue is shown in Fig. 1. The median colour *V* - *R* is 0.49, a value between representative ones for Hubble types *Im* and *Scd*, 0.34 and 0.57, respectively (Fukugita, Shimasaku & Ichikawa 1995).

Global properties of the CUYS catalogue, in terms of *EW* and H α +[NII] fluxes are shown in Figs. 2 and 3, respectively. The median of each distribution is shown together with representative values for the UCM (Gallego et al. 1996) and KR2 surveys. The median values for the CUYS catalogue are between the medians for the other surveys, providing an objective measurement of the *shallowness* of our survey relative to previous ones of similar nature. The limitations in prism dispersion and CCD scale do not allow us to

⁵ Available at <http://www.cida.ve/~abongiov/CUYS/elgcata.txt> in ASCII format.

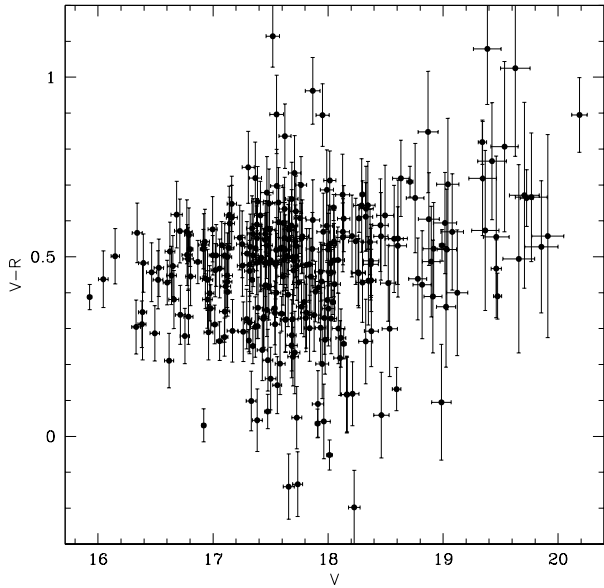


Figure 1. Colour-magnitude diagram for a sample of 314 ELGs in the CUYS list. The median brightness is $V = 17.71$ and the median colour $V - R = 0.49$. This colour is comparable to the colour of local Hubble types *Im* and *Scd* reported by Fukugita, Shimasaku & Ichikawa (1995).

detect ELG candidates with $EW < 30 \text{ \AA}$ (see below). Thus, in this work we detect only the contribution of the most vigorous extragalactic star-forming systems, neglecting the bulk of ELGs with low- EW . Despite this handicap of our survey, we show that it is possible to obtain fair results with these data.

From the original list of ELGs we selected a subset comprised by 273 objects belonging to the connected sky region better sampled in the survey. This subset contains ELG candidates with emission lines blueward of 7750 \AA to avoid confusion with telluric A-band absorption in low resolution spectra. This results in a redshift cut-off of $z \sim 0.14$ for $\text{H}\alpha + [\text{NII}]$ ELG. This subset is denoted hereafter as the Uniform Subset (UnSu).

2.4 Comparison with SDSS results

Taking into account that the CUYS was originally designed to study the properties of the telescope-CCD mosaic-objective-prism combination, a dedicated follow-up spectroscopy of ELG candidates was disregarded, in part due to the availability of SDSS data releases after the first part of the CUYS was finished. We intend to make the best use of our observational effort and to compare the results of the CUYS survey with previous surveys.

The ELG candidates included in the UnSu are represented in the top of Fig. 4 (dots). About 80 per cent of this angular extent overlaps the large sky zone explored by SDSS. From the SDSS2 we extracted common objects (using equatorial coordinates, apparent brightness in R band and redshift as matching parameters) in the overlapping region ($\alpha \leq 236^\circ$) as well as their spectra. We find that all of them (190) are extragalactic emission-line systems (in-

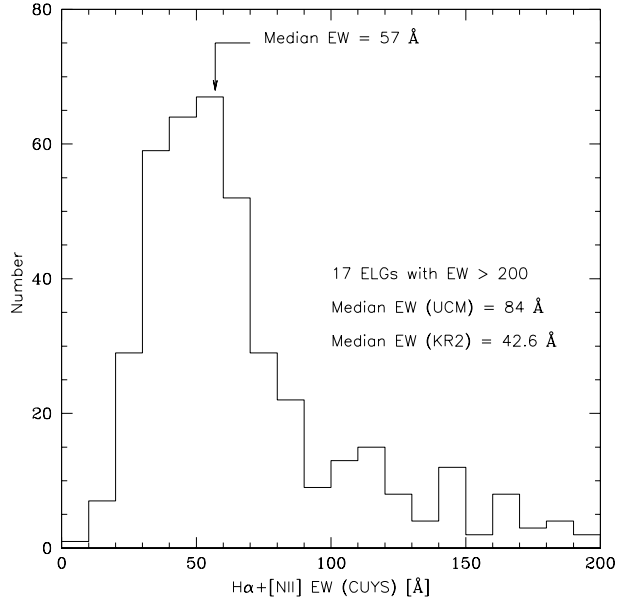


Figure 2. Distribution of $\text{H}\alpha + [\text{NII}]$ reduced equivalent widths for the CUYS ELG candidates. The survey has good sensitivity for $EW \geq 30 \text{ \AA}$. The median values for CUYS, UCM and KR2 are indicated.

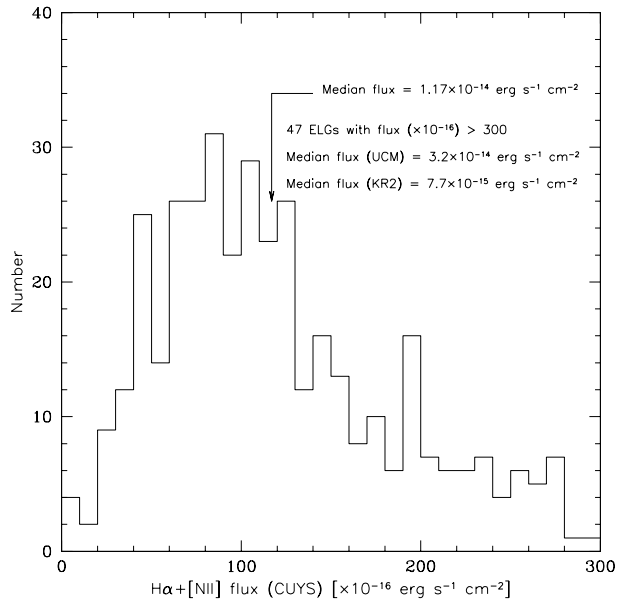


Figure 3. Distribution of $\text{H}\alpha + [\text{NII}]$ fluxes for the CUYS ELG candidates. The median values for CUYS, UCM and KR2 are indicated.

cluding AGN), represented in Fig. 4 by circled dots. The histograms in this figure show the distributions of coordinates difference between CUYS and SDSS2 objects in common: 66% of these differences are below ~ 0.3 arcsec in both coordinates.

There are 46 CUYS objects with $\alpha \leq 236^\circ$ present in the SDSS2 imaging database, but not in the spectroscopic

database. The SDSS2 images of such objects were inspected individually to find the possible reasons for this exclusion. Using the brightness (r_{pet}) distribution of the SDSS2 objects that match with the CUYS ELGs, we find that 16 possibly are too bright to be included in SDSS2 spectroscopic database, 5 objects are too faint and 25 objects are complex (paired) systems. The latter fall in the spectroscopic data hole category. Despite we do not have confirmation about the presence of emission lines in their spectra, these objects are considered hereafter as $\text{H}\alpha + [\text{NII}]$ ELG.

From the perspective of the SDSS2, 90 per cent or more of the CUYS objects can be accepted as reliable ELGs. A comparison of the ELG redshifts and $\text{H}\alpha + [\text{NII}]$ fluxes between the CUYS and the SDSS2 common objects is shown in Fig. 5. The SDSS2 integrated fluxes were obtained from the original spectra degraded to the prism characteristic dispersion with the purpose of integrating the contribution of $\text{H}\alpha$ and $[\text{NII}]$ 6549, 6584 lines into a single line to be fitted as the $\text{H}\alpha + [\text{NII}]$ emission line of the CUYS spectra. The correspondence is evidently quite good, nevertheless the intrinsic error associated with the CUYS absolute flux calculation is between 4 and 8 per cent, whereas the redshift uncertainty is below 0.01. The dispersion in the flux correlation between the SDSS2 and the CUYS common objects, especially those with low $\text{H}\alpha + [\text{NII}]$ flux, could be due to the small and single aperture used in the SDSS spectroscopy defined by the size of their fibers, in contrast with the CUYS. This could explain the slight overestimation of the CUYS flux as compared to SDSS2 $\text{H}\alpha + [\text{NII}]$ flux, below $10^{-14} \text{ erg s}^{-1} \text{ cm}^{-2}$.

On the other hand, if all $\text{H}\alpha + [\text{NII}]$ emission-line systems from the SDSS2 (in the sky zone that overlaps the CUYS) are extracted and analysed, the results are comparable with the CUYS in number, redshift ($z \lesssim 0.15$), $\text{H}\alpha + [\text{NII}]$ fluxes and EW , but only for $EW \geq 30 \text{ \AA}$. Nearly 81% of emission-line systems in SDSS2 (944 in this sky region) have $EW < 30 \text{ \AA}$ (median=16.4 \AA) and the CUYS is insensitive to these objects. In other words, the results obtained by both surveys are nearly identical if we restrict SDSS2 to ELGs with $EW(\text{H}\alpha + [\text{NII}]) \geq 30 \text{ \AA}$.

2.5 Survey Completeness

The completeness of the ELG sample was determined using the V/V_{max} test (Schmidt 1968). A sample is considered *complete* below some apparent magnitude, assuming an uniform distribution of objects, when the average $\langle V/V_{\text{max}} \rangle$, defined by

$$\frac{V}{V_{\text{max}}} = \left[\frac{r}{r_C} \right]^3 = 10^{0.6 \times (m - m_C)} \quad (1)$$

reaches a value of ~ 0.5 . In this equation the subindex C corresponds to the completeness limit for which V/V_{max} is being computed. This test indicates that the CUYS is statistically complete if we include all objects in the UnSu with $m_{L+C} = -2.5 \log(f_{L+C}) - 16.32 \leq 18.05$. This subsample of 183 objects will be called the Complete Subsample (CoSu). The last equation defines an arbitrary magnitude scale $m \equiv m_{L+C}$ as a function of the line + continuum flux f_{L+C} (in $\text{erg s}^{-1} \text{ cm}^{-2}$), and the completeness magnitude was obtained by successive approximations of this expression. This apparent brightness formalism was used originally by Schechter (1976). The zero point of m_{L+C} in this survey was

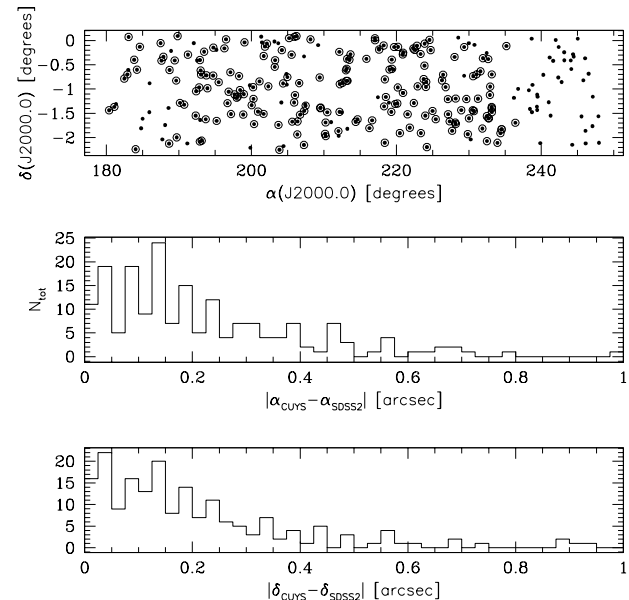


Figure 4. On the top, a map with the CUYS UnSu (273 ELGs, dots). Circled dots (190 objects) are CUYS candidates included in the SDSS2. Objects with $\alpha > 236^\circ$ (38) are not present in the spectroscopic SDSS2 dataset. Single dots with $\alpha \leq 236^\circ$ represent CUYS UnSu objects that do not match SDSS2, mainly because they are possibly too bright to be included in SDSS samples. Distributions in the other two panels correspond to the differences in equatorial coordinates between CUYS (USNO-A V2.0) and SDSS2 astrometry.

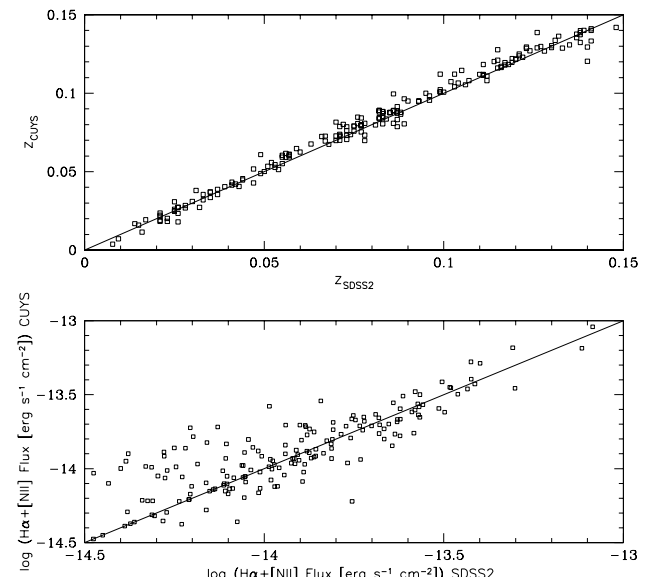


Figure 5. On the top, the redshift (z_{SDSS2}) of SDSS2 objects versus redshift catalogued in our survey (z_{CUYS}). The rms deviation in the horizontal direction is 0.004. In the bottom panel, the comparison between SDSS2 and CUYS $\text{H}\alpha + [\text{NII}]$ fluxes. The rms deviation of CUYS flux is 0.23. In both panels, the straight line has slope=1.

Table 2. $\langle V/V_{max} \rangle$ test data. Column (1) contains limiting magnitude m_{L+C} adopted as described in the text. Column (2) lists the cumulative number of ELGs brighter than m_{L+C} . Column (3) lists the corresponding $\langle V/V_{max} \rangle$ values and column (4), the completeness percentage.

m_{L+C}	Cumulative number	$\langle V/V_{max} \rangle$	Completeness
16.0	4	0.625	100.00
16.1	4	0.544	100.00
16.2	6	0.621	100.00
16.3	7	0.597	100.00
16.4	9	0.625	100.00
16.5	9	0.544	100.00
16.6	12	0.583	100.00
16.7	13	0.545	100.00
16.8	17	0.586	100.00
16.9	24	0.636	100.00
17.0	31	0.642	100.00
17.1	35	0.602	100.00
17.2	43	0.600	100.00
17.3	54	0.609	100.00
17.4	68	0.616	100.00
17.5	88	0.631	100.00
17.6	109	0.621	100.00
17.7	126	0.594	100.00
17.8	141	0.560	100.00
17.9	160	0.541	100.00
18.0	175	0.511	100.00
18.1	190	0.483	97.94
18.2	206	0.461	95.81
18.3	219	0.433	93.60
18.4	230	0.404	90.91
18.5	239	0.375	88.85
18.6	248	0.348	86.71

established using a linear fit to the Johnson R magnitude of ELG candidates. Using this magnitude scale, we performed an independent completeness estimate following Surace & Comte (1998), which apparently is less sensitive to space density fluctuations in the sample. The results agree with those obtained using $\langle V/V_{max} \rangle$: the same completeness limit is reached at $m_{L+C} = 18.15$, with 193 objects. We adopt the $\langle V/V_{max} \rangle$ estimate and the results of the test are given in Table 2.

Concerning the completeness of the survey at the bright end, we are missing a few objects with $m_{L+C} < 15$, whose spectra may appear saturated in our scans. This bias does not affect our conclusions below in a statistical sense. At the faint end, the cause of a possible deficit is discussed in the next section.

2.6 Catalogue Contamination

A source of catalogue contamination is the possible presence in our sample of $z \geq 0.4$ ELGs with emission features different from the $\text{H}\alpha + [\text{NII}]$ blend, which are bright enough to produce good S/N ratio prism spectra. To obtain an idea about the fraction of these objects in the CUYS catalogue we followed the prescription of Jones & Bland-Hawthorn (2001), based on the expected fluxes of the $\text{H}\alpha$, $[\text{OIII}]4959,5007$, $\text{H}\beta$, and $[\text{OII}]3727$ lines, which could eventually be confused with $\text{H}\alpha + [\text{NII}]$ in our spectra. This analysis demonstrates, for example, that at an $\text{H}\alpha$ flux of $\sim 6 \times 10^{-16}$ erg s^{-1} cm^{-2} , the probability of finding objects with $[\text{OIII}]4959,5007$ emission in place of $\text{H}\alpha$ for the CUYS spectral range is ~ 5 per cent. Our estimate for the minimum $\text{H}\alpha$ flux that we detect, at least in the CoSu, is 4.62×10^{-15} erg s^{-1} cm^{-2} , about one order of magnitude higher than the value quoted above. Consequently, there is no evidence of contamination by lines different to the $\text{H}\alpha + [\text{NII}]$ blend in the spectra of the objects that belong to the CUYS catalogue, as it was confirmed using SDSS2 data.

2.7 Spectral Classification of CUYS ELGs

Finally, a description of the CUYS sample would not be complete without including the spectral classification of the galaxies. We have separated the ELGs in three different classes: HII region-like ELGs, SB-like (Starburst) ELGs and AGN or “active galaxies”. HII region-like class corresponds to a synthesis of HIIH and DHIIH types and SB-like class comprises SBN and DANS types, all described by Gallego et al. (1996). This classification was performed only for descriptive purposes and using strictly spectroscopic criteria. Fig. 6 is a representation of the diagnostic diagram $\log([\text{OIII}]5007/\text{H}\beta)$ versus $\log([\text{NII}]6583/\text{H}\alpha)$, useful according to Veilleux & Osterbrock (1987) for spectral classification of ELGs. Data for these emission lines were extracted from 180 matched SDSS2 spectra with measurable diagnostic lines, using the IRAF task `splot`. The objects whose spectra are analyzed here belong to the UnSu, therefore the work done here do not implies the extraction of *all* AGNs present in the CoSu, but to have a very clear idea about the *fraction* of different spectral classes of ELGs present in our largest subsample. The analysis of the SDSS2 matched spectra reveals that ~ 18 per cent of the CUYS sample is composed by AGN (squares). From the 143 star-forming galaxies plotted, 36 are HII region-like ELGs (triangles) and 107 are SB-like (circles).

We have overplotted on the the diagnostic diagram a sequence of models for star-forming galaxies (Magris, Binette & Bruzual 2003), to obtain an accurate idea about metallicity and burst age of surveyed ELGs. The solid line segments join models of constant metallicity, whereas dotted lines join models of equal ionization parameter.

The sequences correspond to an instantaneous burst of star formation, with age between 0 and 2 Myr. We observe that 91 per cent of the star-forming galaxies sample lies on a locus with a metallicity between 0.4 and $1 \times Z_\odot$. The remaining objects (HII region-like ELGs) have lower metallicities. The broad distribution of star-forming galaxies in this diagram can be understood as due to dispersion in the age of the burst.

3 CUYS $\text{H}\alpha$ LUMINOSITY FUNCTION IN THE LOCAL UNIVERSE

The ELG CoSu was used to derive an $\text{H}\alpha$ Luminosity Function (LF) whose integral value represents an estimate of ρ_{SFR} in the Local Universe.

To fit the LF we compute the number Φ of galaxies per unit volume and per unit $\text{H}\alpha$ -luminosity interval $0.4 \log L(\text{H}\alpha)$, given by

$$\Phi[\log L(\text{H}\alpha)] = \frac{4\pi}{\Omega} \sum_i \frac{1}{V_i^{max}}, \quad (2)$$

where Ω is the surveyed solid angle (~ 0.046 str) and V_i^{max} is the volume enclosed by a sphere of radius equal to the maximum distance the galaxy could be from the i th-object and still be detected in the survey (Schechter 1976). The sum is performed over all the objects whose luminosity falls in the interval $L(\text{H}\alpha) \pm 0.5 \Delta \log L(\text{H}\alpha)$.

Following the reasoning above, the Schechter function can be rewritten as

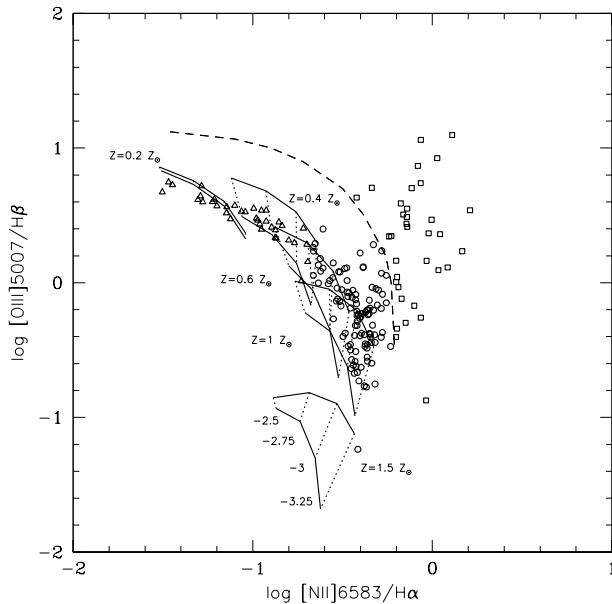


Figure 6. Diagnostic diagram $\log([OIII]5007/H\beta)$ versus $\log([NII]6583/H\alpha)$ for 180 CUYS ELGs with counterparts in the SDSS2 sample. Using the prescription of Veilleux & Osterbrock (1987) and spectroscopic criteria referred in the text, nearly 80 per cent of the CUYS sample can be regarded as HII region-like ELGs (triangles) and SB-like ELGs (circles). The remaining objects were classified as AGN (squares). Solid line segments represent a sequence of models for star-forming galaxies according to Magris, Binette & Bruzual (2003), as described in the text.

$$\Phi[\log L(H\alpha)] d\log L = \phi(L)dL, \quad (3)$$

where $\phi(L)dL \equiv \phi^*(L/L^*)^\alpha \exp(-L/L^*)d(L/L^*)$. In the V_i^{max} method, galaxies are assumed to be distributed homogeneously and, for this reason, its great advantage is simplicity. Nevertheless, the data were subject to other classical fitting schemes (Felten 1977, Eales 1993) and the results agree, within errors, with the ones obtained from the V_i^{max} method.

We use a median value for the ratio $(H\alpha + [NII])/H\alpha = 1.3$ derived from the SDSS2 galaxies in common with our sample to correct objective-prism $H\alpha + [NII]$ fluxes for the contribution by [NII]. This value, derived from original and degraded resolution SDSS2 spectra, is consistent with the 1.33 value reported by Kennicutt (1983) and Gallego et al. (1997), which is widely used in the literature for local ELGs.

$L(H\alpha)$ for each galaxy was dust corrected stochastically via 10^4 Monte Carlo simulations of intrinsic reddening $A(H\alpha)$, whose distribution is represented on the top of Fig. 7. The calculation of the reddening is based on the theoretical Balmer decrement $H\alpha/H\beta = 2.86$ (Osterbrock 1989), assuming case B recombination, $T_e = 10^4$ K and $n_e = 10^2 \text{ cm}^{-3}$; in the case of AGNs, we used $H\alpha/H\beta = 3.10$. We take the Withford extinction curve that satisfies $k(\lambda) = A_\lambda/E(B-V)$ and use the Seaton (1979) law, which gives $k(H\alpha) = 2.49$. The $A(H\alpha)$ distribution behaviour is a polynomial fit of the binned inverse distribution function.

Unlike the alternative $LF(H\alpha)$ calculation that follows in this section, we assume that the $A(H\alpha)$ correction prob-

ability for each ELG in the Monte Carlo realisations is, in principle, the same. Obviously, the $A(H\alpha)$ correction likelihood for each galaxy is conditioned by the shape of the distribution function represented on the top of Fig. 7. The intrinsic reddening $A(H\alpha)$ was calculated using the $E(B-V)$ colour excess and *observed* intensity ratios $H\alpha_o/H\beta_o$ from 165 SDSS2 spectra corresponding to ~ 61 per cent of the UnSu. In the simulations we also include the error distribution functions for galaxy $H\alpha$ flux and redshift.

The three lower panels of Fig. 7 contain the Schechter function parameters distributions ($\log \phi^*$, α and $\log L^*$, respectively) for the LF obtained from Monte Carlo experiments (99.5 per cent confidence level). Inside each distribution the median and its deviation ($1-\sigma$) is represented as a bar. These $1-\sigma$ deviations were adopted as the corresponding error parameter in this approach, whose representation is shown in Fig. 9 (solid thick line).

We also implemented a simpler form to correct the $L(H\alpha)$ by reddening. It consists in deriving a correlation of $E(B-V)$ with absolute magnitude M_B just as presented by Jansen, Franx & Fabricant (2001), but using the data from the 165 SDSS2 galaxy spectra. A linear fit between these variables is shown in Fig. 8. The rms of the residuals reaches ~ 0.2 mag in color excess, which represents a $H\alpha$ extinction of about 0.6 mag. We agree with these authors in the scatter in this trend. In spite of this, the correlation was used to correct $L(H\alpha)$ for each galaxy individually and the parameters of the LF($H\alpha$) were calculated using a Marquardt-Levenberg least-squares fit: $\log L^* = 42.06 \pm 0.14$, $\alpha = -1.35 \pm 0.16$ and $\log \phi^* = -3.12 \pm 0.25$. This LF($H\alpha$) is represented in Fig. 9 by a solid thin line. The number distribution of CoSu objects used in this LF calculation is shown in the bottom of the figure. The error bars in the points are Poissonian errors.

Despite the relative shallowness of the CUYS, the parameter values and associated errors obtained with both approaches are acceptable. The stochastic method favours slightly the fainter luminosities whereas the alternative approach, the brighter ones. We adopt the parameters resulting from stochastic approximation to the LF($H\alpha$) calculation problem because it takes into account the error distribution functions for galaxy $H\alpha$ flux and redshift. The resulting LF parameters from this method are listed in Table 3 together with values for different surveys performed after the UCM survey (Gallego et al. 1995) for comparison purposes, and all of them shown in Fig. 9. A number defect in CUYS LF($H\alpha$) at fainter luminosities is evident when it is compared with previous estimations. This is evidently related to the CUYS selection effects, mainly the absence of ELGs with $EW < 30\text{\AA}$ and, to a smaller extent, the exclusion of point-like ELGs as part of the data reduction process.

Given a Schechter function approximation to the $H\alpha$ luminosity distribution in the volume of local universe considered, the integrated $H\alpha$ -luminosity $\mathcal{L}(H\alpha)$ has the value

$$\mathcal{L}(H\alpha) = \int_0^\infty \phi(L) L dL = \phi^* L^* \Gamma(2 + \alpha), \quad (4)$$

which is given in the last line of the Table 3. All the estimates in Table 3 seem very similar, the CUYS $\mathcal{L}(H\alpha)$ is the smallest value, but it is very close to the estimate of Gallego et al. (1995). Probably, our number defect of ELGs is real in the volume of universe surveyed. We need to stress

Table 3. CUYS LF(H α) and related data compared with earlier works as tabulated in Nakamura et al. 2004 ($h = 1$). The $\log \mathcal{L}(\text{H}\alpha)$ value for the CUYS *includes* the contribution by AGNs.

	Gallego et al. (1995)	Tresse & Maddox (1998)	Sullivan et al. (2000)	Nakamura et al. (2004)	CUYS
Survey area	471.4 deg 2	500 arcmin 2	~ 10 deg 2	229.7 deg 2	151.1 deg 2
Mean redshift	~ 0.025	0.21	0.15	0.054	0.081
Size of the sample	176	110	159	665	183
$\log L^*$	41.56 ± 0.08	41.61 ± 0.13	42.11 ± 0.14	41.68 ± 0.10	41.74 ± 0.16
α	-1.3 ± 0.2	-1.35 ± 0.06	-1.62 ± 0.10	-1.43 ± 0.10	-1.32 ± 0.16
$\log \phi^*$	-2.3 ± 0.2	-2.09 ± 0.09	-3.04 ± 0.20	-2.56 ± 0.30	-2.72 ± 0.24
$\log \mathcal{L}(\text{H}\alpha)$	39.38 ± 0.04	39.66 ± 0.04	39.43 ± 0.06	39.31 ± 0.04	39.23 ± 0.07

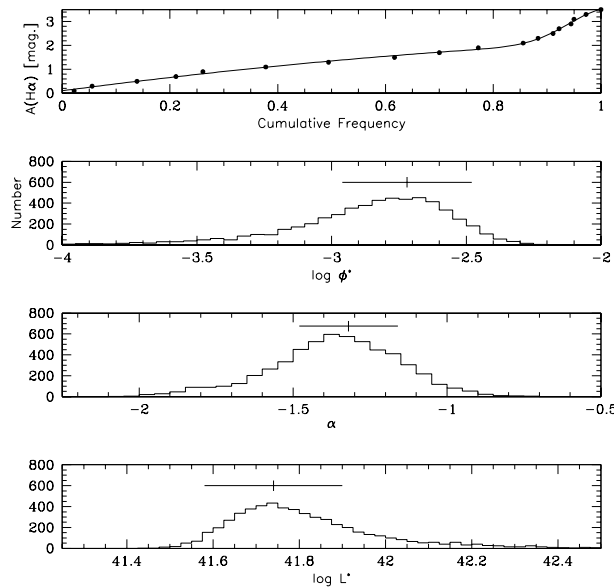


Figure 7. In the top panel the distribution of reddening in H α from the SDSS2 selected sample (165 ELGs) in common with the CUYS UnSu. The other plots contain the distribution of the Schechter function parameters obtained via Monte Carlo experiments, with the restrictions explained in the text.

here again that the CUYS value for $\mathcal{L}(\text{H}\alpha)$ is valid for star-forming galaxies with $EW(\text{H}\alpha + [\text{NII}]) > 30\text{\AA}$.

We translate the integrated H α -luminosity $\mathcal{L}(\text{H}\alpha)$ into a SFR density via the transformation

$$\mathcal{L}(\text{H}\alpha) = 1.21 \times 10^{41} \rho_{\text{SFR}}, \quad (5)$$

which is taken from Magris, Binette & Bruzual (2003), assuming a Salpeter IMF from 0.1 to $125 M_{\odot}$, and solar stellar and gas metallicity. Consequently, the estimate from the CUYS is (statistical error)

$$\rho_{\text{SFR}} = 0.014 \pm 0.002 h M_{\odot} \text{ yr}^{-1} \text{ Mpc}^{-3}. \quad (6)$$

Obviously, this quantity must be regarded with caution. In the CUYS LF calculation we *included* AGNs. As it was explained in the previous section, we are sure about the *fraction* of these objects in the sample, but not on their identification all over the catalogue. We preferred to leave them in the sample rather than extract only a fraction. Additionally, we do not correct the H α flux for stellar absorption. This correction is really negligible given the EW val-

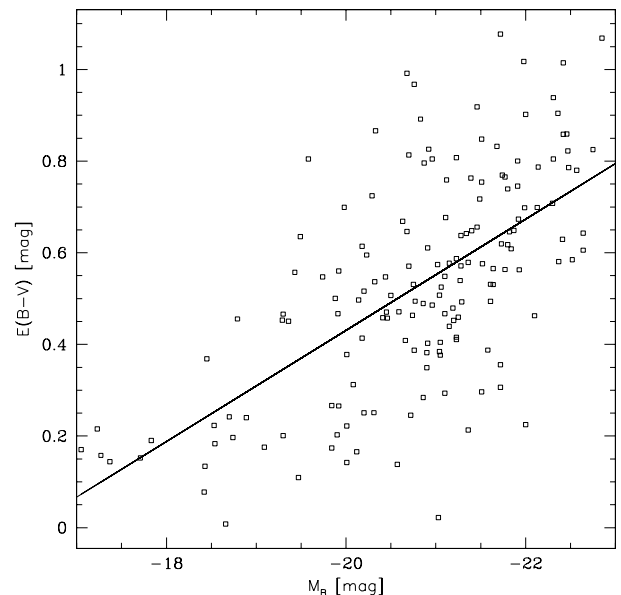


Figure 8. Relation between colour excess $E(B - V)$ and absolute magnitude M_B for the 165 CUYS objects that match SDSS2 galaxies. The linear fit (residual 0.19 mag rms) was used to calculate $A(\text{H}\alpha)$ for each galaxy of the UnSu before performing the LF(H α) alternative estimation.

ues considered here. Thus, if we use the table with LF(H α) systematic errors calculated by Nakamura et al. (2004), the CUYS ρ_{SFR} value has a combined systematic error of at most $\pm 0.003 h M_{\odot} \text{ yr}^{-1} \text{ Mpc}^{-3}$ due to neglecting stellar absorption and the AGNs inclusion.

4 SPATIAL DISTRIBUTION OF CUYS ELG

The CUYS provides a good opportunity to obtain information about the spatial distribution of ELGs with high SFR via 2-point correlation functions and to establish a preliminary determination of the ELG sample bias compared to a recent set of “normal” or “quiescent” galaxies in the same spatial volume. Below we study the relation between star formation and environment conditions from three different perspectives.

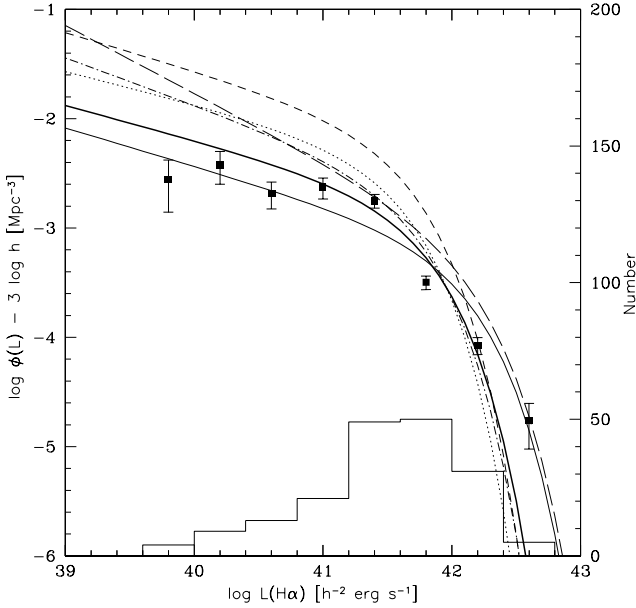


Figure 9. LF(H α) determinations for the surveys listed in Table 3. The solid thick line corresponds to the CUYS LF corrected for dust and errors via Monte Carlo experiments. The solid thin line that fits the discrete values is the CUYS LF with dust correction using Jansen, Franx & Fabricant (2001) prescription as is described in the text. Bars are Poissonian errors. On the bottom of the figure is the number distribution of CoSu ELGs used in this LF calculation. The dotted line corresponds to the Gallego et al. (1995) LF, the short-dashed line to Tresse & Maddox (1998), the long-dashed line to Sullivan et al. (2000) and the dot-dashed line to the Nakamura et al. (2004) fit.

4.1 Reference Catalogue and Qualitative Environmental Effects

First, we wish to compare the CUYS ELG spatial distribution with a deeper sample of galaxies than the usual bright galaxy catalogues. As a first reference catalogue (RC1) we use a subset of 9,364 quiescent galaxies from the spectroscopic sample of SDSS2, with $R \leq 18.15$ and $z \leq 0.14$ as the selection criteria. The completeness limit of the SDSS galaxy catalogue to $z \sim 0.1$ is $r_{\text{pet}} \leq 17.8$ (Blanton et al. 2003). This selection resembles the CUYS sample in terms of limiting flux and volume of universe. From the RC1 we extracted galaxies that match the CUYS CoSu. Unfortunately, the angular overlap between both catalogues forced us to limit the CUYS CoSu to 132 deg 2 (161 objects). A representation of the RC1 and the CUYS CoSu (trimmed) in velocity space can be seen in Fig. 10. It is easy to distinguish density enhancements in the distribution of RC1 galaxies in redshift space. To obtain an estimate of the RC1 galaxy clustering, we use the Huchra & Geller (1982) *Friends-of-Friends* (*FoF*) algorithm for group and cluster finding in magnitude-limited samples of galaxies (with $D_0 = h^{-1} 0.4$ Mpc, the projected separation chosen at some fiducial redshift and $V_0 = 350$ km s $^{-1}$, adopted as parameters after various trials). We find 307 groups with between 5 and 350 members each. We discarded groups with less than 5 members. Once the group and cluster catalogue was constructed, we divided the CUYS CoSu in two subsets: *grouped*, associated with one or more quies-

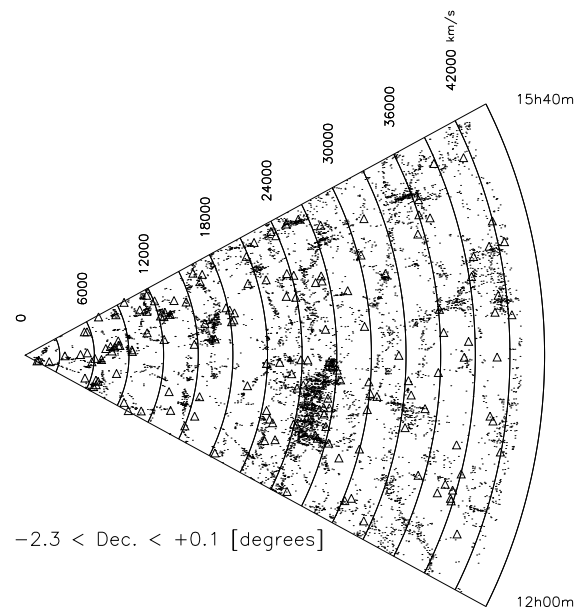


Figure 10. Pie diagram with RC1 galaxies (small dots; 9,364 objects) and CUYS CoSu ELG (triangles; 161 objects) that lie in the same volume.

cent galaxy groups (17 objects), and *isolated* ELGs (144 objects). We find a ratio $SFR_{\text{isolated}}/SFR_{\text{grouped}} = 1.4 \pm 0.3$. If we use the CfARS catalogue from Huchra et al. (2001, private communication) for double-checking this result, this ratio reaches 2.1 ± 0.5 . The CfARS catalogue is complete to $B = 15.24$ and the sample used for our purposes has 669 galaxies. It seems clear that the average star formation in low density environments is about a factor of 1.5 to 2 greater than in group and cluster regions, at least when galaxies with copious star formation are used as tracers of the SFR.

4.2 2-point Correlation Functions

We used the RC1 and the CUYS CoSu (trimmed) sets of galaxies to examine clustering properties by means of auto-correlation algorithms in redshift space. With this purpose, we adopt the correlation function (CF) formalism proposed by Hamilton (1993). This correlation function estimator is defined by

$$\xi(s) = \frac{\langle NN(s) \rangle \langle RR(s) \rangle}{\langle NR(s) \rangle^2} - 1, \quad (7)$$

where $NN(s)$ is the number of catalogue galaxies in the interval $[s, s+ds]$, $RR(s)$ is the number of pairs in the same interval in the random catalogue (~ 20 times larger than the size of data sample), and $NR(s)$ is the number of pairs in the combined sample with this separation. The angular brackets in this equation denotes average over all pairs separated by s in the galaxy sample.

The error in the CF estimate is defined as the standard deviation at each point where the CF was measured. To diminish boundary effects, the RC1 sample was enhanced by 2 degrees in angular dimension and the random catalogues were re-sampled in each simulation.

Table 4. Correlation function parameters ($h = 1$).

Sample	s_0 [Mpc]	γ	scale range [Mpc]
CUYS CoSu	6.87 ± 0.79	1.68 ± 0.22	$3.5-8.5$
SDSS2	6.08 ± 0.05	1.26 ± 0.06	$1.5-10.5$
SDSSER (2002)	6.10 ± 0.03	1.75 ± 0.03	$0.1-16.0$

It was possible to obtain positive values of the 2-point CF for the CUYS CoSu only when $s > h^{-1} 1$ Mpc. This indicates that the ELGs are anti-clustered, or that they are arranged regularly in redshift space at smaller scales. The galaxy correlation function can be approximated by a power-law (Peebles 1980)

$$\xi(s) = \left(\frac{s}{s_0} \right)^{-\gamma}, \quad (8)$$

where s_0 is the correlation length (defined as $\xi(s_0) \equiv 1$) and γ is the power-law slope. The top panel of Fig. 11 shows estimates of the redshift space 2-point CF for each sample. The results of the fits are given in Table 4.

The points in Fig. 11 are distributed in $1 h^{-1}$ Mpc bins reaching up to $\sim 11 h^{-1}$ Mpc, where the known shoulder in $\xi(s)$ is not yet appreciable. Moreover, beyond this limit, the CF determination for the CUYS CoSu was unacceptably noisy. We include for reference in Table 4 and Fig. 11 the fit obtained by Zehavi et al. (2002) for general galaxy clustering in the SDSS Early Release (SDSSER). A power-law fitting for the CUYS CoSu was possible only in the scale range $3.5-8.5 h^{-1}$ Mpc.

It is evident that the clustering amplitude in this scale range is similar in the 3 samples. ELGs appear to be practically as clustered as SDSS2 galaxies. On the other hand, below $3.5 h^{-1}$ Mpc, ELGs seem 2 to 5 times less clustered than quiescent galaxies. The bias pictured in the bottom panel of Fig. 11, defined as the ratio $\xi_{\text{CUYS}}/\xi_{\text{SDSS2}}$, shows an asymptotical behaviour on scales $s > 3 h^{-1}$ Mpc with an apparent shoulder on smaller scales that should be confirmed with larger ELG samples.

4.3 Environment and SFR density

As indicated in the introduction to this paper, a recent and detailed analysis about the effect of environment on the star formation activity in the local universe was published by Gómez et al. (2003). They found that the SFR in nearby galaxies is strongly correlated with the *projected* galaxy density in at least three different (and complementary) ways: (a) the decrease of the overall SFR distribution in dense environments compared to the field population; (b) this effect is most noticeable for the stronger star-forming galaxies; (c) the existence of a characteristic density in the density-SFR relation at a local galaxy density of $\sim 1 h_{75}^2$ Mpc $^{-2}$.

Despite the limitations imposed by the absence of a morphological classification of CUYS CoSu ELGs and the relative small size of this subsample, we have extracted additional information about the effects of environment on SFR density. The availability of a characteristic correlation length s_0 for the CUYS ELGs give us the opportunity to use a different approach in the quantification of the environmental effects discussed in the section 4.1. The distance s_0 sepa-

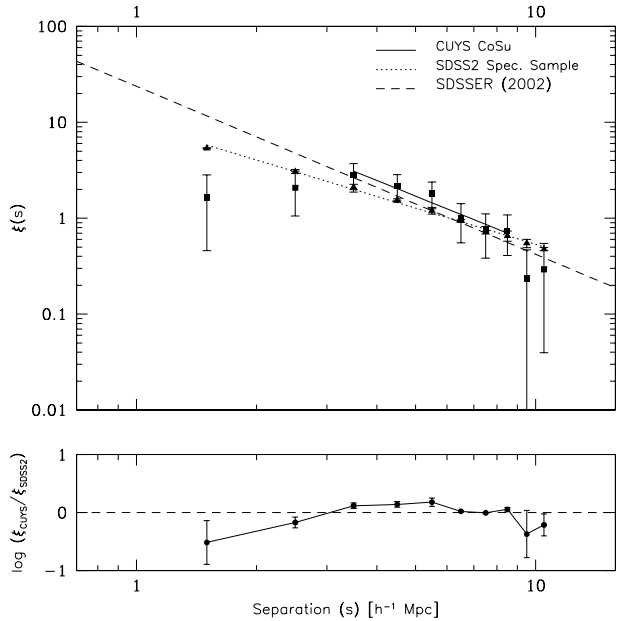


Figure 11. The top panel shows the redshift space 2-point correlation function for the CUYS CoSu (squares) and the SDSS2 sample (triangles). The bars show the standard deviation. The continuous line represents the CUYS CF in the scale range $3.5-8.5 h^{-1}$ Mpc. The dotted line is the fit to CF for the SDSS2 sample and the dashed line is a reference from the SDSSER (2002). The bottom panel shows the bias between the CUYS CoSu and the SDSS2 sample correlation function, defined as the quotient of both quantities.

rates the regime of large spatial density fluctuations from the regime of small fluctuations. The latter can be interpreted as a homogeneous galaxy distribution, but this is a current topic of debate (Gaite, Domínguez & Pérez-Mercader 1999).

We now use the CUYS CoSu correlation length s_0 as a characteristic radius to compute the environment galaxy density in the redshift space. This corresponds to an *ELG-centric* perspective of the environmental effects on star formation. We calculate the average density of galaxies, Δ , and the star formation rate density ρ_{SFR}^* inside spheres of radius s_0 centered in each galaxy of the CUYS CoSu, integrating the $L(\text{H}\alpha)$ of the galaxies involved in each volume. The results are expressed as a distribution function in Fig. 12. The inverse proportionality between the environment and the SFR spatial density is not only evident, but a power-law behaviour describes rather well this phenomenon. The best-fit to the distribution is

$$\rho_{\text{SFR}}^* (h = 1) = \left(\frac{\Delta}{1.47(\pm 0.19) \times 10^{-4}} \right)^{1.28 \pm 0.11}. \quad (9)$$

This is the first reported quantitative parametrisation of the SFR density dependence on the average *spatial* density of galaxies based on ELGs with vigorous star formation. We have deliberately omitted the separation between dense environments and field populations of ELGs to obtain a perspective about the *continuum* without “breaks” that seems to link both variables at a distance scale comparable to s_0 . An interesting future work could be to profit from the SDSS recent releases to explore more deeply the spatial environ-

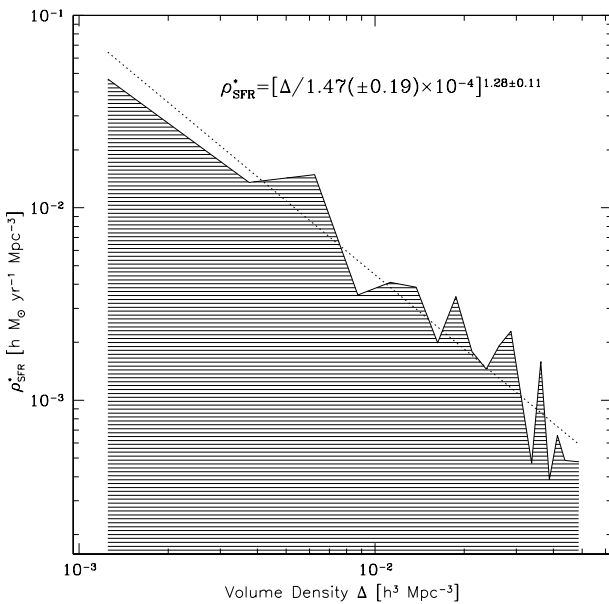


Figure 12. Relation between the volume density of galaxies and the star formation rate density inside spheres of radius equal to the correlation length s_0 in redshift space derived from the 2-point correlation function fitted to the CUYS CoSu sample.

mental effects on the SFR, using perhaps other descriptors of galaxy clustering.

5 CONCLUSIONS

In this paper we present the basic properties of the objective-prism CUYS for ELGs, with special emphasis on the $z \leq 0.14$ sample. The size, covered sky area, and $\text{H}\alpha + [\text{NII}]$ flux distribution, make our survey competitive with other modern ELG surveys. Technical limitations forced us to search and find ELGs with $EW(\text{H}\alpha) > 30 \text{ \AA}$. Thus, all the work in this paper refers to local galaxies with vigorous star formation. Our main results can be summarized as follows:

- Objective-prism searches for ELGs provide a productive and cheap method to generate large catalogues of local SB-like, HII region-like and active galaxies. We used the driftscan technique, coadding 1-dimensional reduced spectra from multiple scans of the same region of the sky.
- The typical colour of ELGs in our sample is $V - R = 0.49$, comparable to the mean colour of local Hubble types *Im* and *Scd*. The analysis of the diagnostic diagram for spectral classification reveals that more than 80 per cent of the CUYS ELGs can be considered star-forming galaxies. From this fraction, nearly 75 per cent is dominated by SB-like ELGs. Photoionization models imply that these galaxies have metallicities between 0.4 and $1 \times Z_{\odot}$ with instantaneous bursts of star formation aged less than 2 Myr.
- Compared with the LF($\text{H}\alpha$) derived from deeper surveys, the CUYS LF($\text{H}\alpha$) shows good agreement with previous results except in the low $\text{H}\alpha$ luminosity region, where we find a small deficit attributed to the survey selection effects. Nevertheless the star formation rate density that we calculate is in agreement with values reported in the literature.

- On average, the SFR for galaxies associated with groups/clusters of quiescent galaxies is 0.5 to 0.7 times the value for isolated ELGs. The fraction of ELGs regarded as *grouped* versus *isolated* is 0.1; additionally, the mean density ratio between star-forming and quiescent galaxies is on the order of ~ 2.5 . Thus, it is clear that ELGs avoid dense regions of quiescent galaxies.

- ELG clustering is statistically indistinguishable from quiescent galaxy grouping in redshift space scales from 3.5 to $8.5 h^{-1} \text{ Mpc}$. Between ~ 1 and $3 h^{-1} \text{ Mpc}$, ELGs are 2 to 5 times less clustered than quiescent galaxies, whereas below $1 h^{-1} \text{ Mpc}$ (~ 1 Abell radius) in redshift space, ELGs are anti-clustered or they are arranged regularly. This result is in agreement with the hierarchical galaxy formation scenario. Perhaps today ELGs are isolated systems that have not yet started the merging process. Conversely, merged galaxies that formed isolated luminous galaxies or today cluster galaxies, have been depleted of enormous amounts of gas and they show today few star formation events.

- Finally, we propose a parametrization of the relation between SFR density and environment density. As far as this survey is concerned, there seems to exist a continuum dependence between these variables which can be described by a power-law.

ACKNOWLEDGMENTS

We are especially grateful to CIDA colleagues who have participated in different discussions about topics directly involved in this paper. Special thanks to the night assistants O. Contreras, F. Moreno, R. Rojas and U. Sánchez and the professional observers L. Romero and D. Herrera of the Venezuelan National Astronomical Observatory for their constant effort.

We also acknowledge the useful suggestions from an anonymous referee. The alternative calculation of the LF($\text{H}\alpha$) using an extinction correction estimated from a correlation between M_B and $E(B - V)$ is included in the referee's recommendations.

The observations reported in this paper were done under the Scientific and Academic Collaboration Agreement signed between the Universidad Complutense de Madrid (UCM), España, and the Centro de Investigaciones de Astronomía "Francisco J. Duarte" (CIDA), Venezuela, in force since 1996 until end of 1999.

Funding for the Sloan Digital Sky Survey (SDSS) has been provided by the Alfred P. Sloan Foundation, the Participating Institutions, the National Aeronautics and Space Administration, the National Science Foundation, the U.S. Department of Energy, the Japanese Monbukagakusho, and the Max Planck Society. The SDSS Web site is <http://www.sdss.org/>. The SDSS is managed by the Astrophysical Research Consortium (ARC) for the Participating Institutions. The Participating Institutions are The University of Chicago, Fermilab, the Institute for Advanced Study, the Japan Participation Group, The Johns Hopkins University, Los Alamos National Laboratory, the Max-Planck-Institute for Astronomy (MPIA), the Max-Planck-Institute for Astrophysics (MPA), New Mexico State University, University of Pittsburgh, Princeton University, the

United States Naval Observatory, and the University of Washington.

A.B. acknowledges R. Guzmán (University of Florida, USA), A. Parravano (Universidad de Los Andes, Venezuela), M. Bautista (Instituto Venezolano de Investigaciones Científicas), M. Bessega (Universidad Central de Venezuela), J. Bergamaschi (Observatorio Cagigal, Caracas), who provided useful advice on the analysis of survey results.

A.B. also acknowledges financial support from the Fondo Nacional de Ciencia, Tecnología e Innovación, Ministerio de Ciencia y Tecnología, Venezuela.

REFERENCES

Abazajian K. et al., 2003, AJ, 126, 2081.

Alonso O., García-Dabó C.E., Zamorano J., Gallego J., Rego M., 1999, ApJS, 122, 415.

Bahcall J.N., Soneira R.M., 1980, ApJS, 44, 73.

Baltay Ch. et al., 2002, PASP, 114, 780.

Blanton M. et al., 2003, ApJ, 592, 819.

Crawford D.F., 1995, ApJ, 441, 488.

Dressler A., Thompson I.B., Shectman S.A., 1985, ApJ, 288, 481.

Eales S., 1993, ApJ, 404, 51.

Felten J.E., 1977, AJ, 82, 861.

Fukugita M., Shimasaku K., Ichikawa T., 1995, PASP, 107, 945.

Gaite J., Domínguez A., Pérez-Mercader J. 1999, ApJ, 522L, 5

Gallego J., Zamorano J., Aragón A., Rego M. 1995, ApJ, 455L, 1.

Gallego J., Zamorano J., Rego M., Alonso O., Vitores A., 1996, A&AS, 120, 323.

Gallego J., Zamorano J., Rego M., Vitores A., 1997, ApJ, 475, 502.

Gisler G.R., 1978, MNRAS, 183, 633.

Gómez P. et al., 2003, ApJ, 584, 210.

Gronwall C. et al., 2004, AJ, 127, 1943.

Hamilton A.J.S., 1993, ApJ, 417, 19.

Huchra J., Geller M., 1982, ApJ, 257, 423.

Irwin M., 1990, MNRAS, 243, 692.

Jansen R.A., Franx M., Fabricant D., 2001, ApJ, 551, 825.

Jones D.H., Bland-Hawthorn J., 2001, ApJ, 550, 593.

Kennicutt R., 1983, ApJ, 272, 54.

Lewis I. et al., 2002, MNRAS, 334, 673.

MacAlpine G.M., Smith S.B., Lewis D.W., 1977, ApJS, 35, 197.

McGraw J.T., Cawson M.G.M., Keane M.J., 1986, Proc. SPIE, 627, 60.

Magris G., Binette L., Bruzual G., 2003, ApJS, 149, 313.

Markarian B.E., Stepanian D.A., Erastova L.K., 1986, Afz, 25, 345.

Monet D. et al., 1998, VizieR On-line Data Catalog: I/252. Originally published in: U.S. Naval Observatory Flagstaff Station (USNOFS) and Universities Space Research Association (USRA) stationed at USNOFS.

Nakamura O., Fukugita M., Brinkmann J., Schneider D.P., 2004, AJ, 127, 2511.

Osterbrock D., 1989, *Astrophysics of Gaseous Nebulae and Active Galactic Nuclei*, University Science Books, California, USA.

Peebles P.J.E., 1980, *The Large Scale Structure of the Universe*, Princeton University Press, Princeton, USA.

Popescu C.C., Hopp U., Hagen H.J., Elsaesser H., 1996, A&AS, 116, 43.

Popescu C.C., Hopp U., Elsaesser H., 1997, A&A, 325, 88.

Pesch P., Sanduleak N., 1983, ApJS, 51, 171.

Sabbe C.N., 1999, ADASS, 8, 207.

Sabbe C.N. et al., 2001, ApJ, 548, 585.

Seaton M.J., 1979, MNRAS, 187, 73.

Salzer J., 1989, ApJ, 347, 152.

Schechter P., 1976, ApJ, 203, 297.

Schmidt M., 1968, AJ, 151, 393.

Schneider D.P., Schmidt M. and Gunn J.E., 1994, AJ, 107, 1245.

Sullivan M. et al., 2000, MNRAS, 312, 442.

Surace G., Comte C., 1998, A&AS, 133, 171.

Tresse L., Maddox S.J., 1998, ApJ, 495, 691.

Ugryumov A.V. et al., 1999, A&AS, 135, 511.

Veilleux S., Osterbrock D.E., 1987, ApJS, 63, 295.

Vivas A.K. et al., 2004, AJ, 127, 1158.

Wasilewski A., 1983, ApJ, 272, 68.

Zamorano J. et al., 1994, ApJS, 95, 387.

Zehavi I. et al., 2002, ApJ, 571, 172.